Predictive Control for Real-Time Frequency Regulation and Rotational Inertia Provision in Power Systems

Andreas Ulbig, Tobias Rinke, Spyros Chatzivasileiadis and Göran Andersson

Abstract— This paper presents real-time optimal control schemes for regulating grid frequency and providing rotational inertia in power systems, two control problems with fast dynamics on the time-scale of milliseconds. Both control problems have received wide attention in recent years due to rising shares of variable renewable energy sources (RES) and the thereby arising challenges for power system operation.

The presented control schemes are based on explicit model predictive control (MPC), which allows to directly incorporate operational constraints of power system units, i.e. ramp-rate, power rating and energy constraints, and to achieve real-time tractability while keeping the online computation effort low. Simulations, including a performance comparison with traditional frequency control, are presented.

I. Introduction

In this paper we present real-time optimal control schemes for regulating grid frequency and providing grid frequency inertia based on a explicit model predictive control (MPC). Both control problems receive wide attention due to the rapidly growing shares of variable renewable energy sources (RES), i.e. wind turbines and PV units, and the thereby arising challenges for power system operation, notably faster frequency dynamics due to reduced rotational inertia.

The control objective of frequency regulation is to minimize the frequency deviation Δf from the nominal grid frequency f_0 (50 or 60 Hz depending on region).

Rotational inertia provision, i.e. increasing the inertia constant H, minimizes the frequency rate of change $\Delta \dot{f}$ in case of power deviations. This renders power system frequency dynamics more benign, i.e slower, and thus increases the available response time to react to fault events such as line losses, power plant outages or large-scale set-point changes of either generation or load units.

The choice of MPC as a control approach is motivated by its capability to incorporate operational constraints of power systems directly in the controller design. Explicit MPC allows the shifting of most of the computational effort offline, thus enabling real-time tractability of MPC schemes for systems with very fast dynamics on the time-scale of milliseconds and keeping online computation requirements low.

A. Ulbig, S. Chatzivasileiadis and G. Andersson are with the Power Systems Laboratory, Department of Electrical Engineering, ETH Zurich, 8092 Zurich, Switzerland.
Email: ulbig | spyros | andersson@eeh.ee.ethz.ch

T. Rinke completed his master thesis at the ETH Zurich Power Systems Laboratory in 2010–11. Email: tobias.rinke@gmail.com

The presented control schemes enable the provision of two crucial ancillary services, frequency control and rotational inertia provision, using *any* generic power system unit for which only the relevant operational constraints, power ramp rate (ρ), power rating (π) and – in case of storage units – also energy storage (ϵ), need to be known.

The paper is organized as follows: In Section II current trends and challenges in power systems operation, which serve as the paper's motivation are presented. Section III explains the dynamics of grid frequency and inertia and the corresponding control problems. Section IV introduces MPC. Section V presents formulation, implementation and simulation results of the proposed MPC-based control schemes for frequency control and inertia provision along with a performance comparison to traditional frequency control based on P/PI controllers.

II. Challenges in Power System Operation

Traditionally, power system operation is based on the assumption that electricity generation, in the form of thermal power plants, reliably supplied with fossil or nuclear fuels, or hydro plants, is fully dispatchable, i.e. controllable, and involves rotating generators. Via their stored kinetic energy they add rotational inertia, an important property of frequency dynamics and stability.

Large-scale deployment of RES generation, notably in the form of wind turbines and photovoltaic (PV) units, has led to significant shares of variable, non-controlled power in-feed in power systems. State-of-the-art wind turbine systems are often grid-connected via AC-DC-AC converters, thus canceling (most of) the electro-mechanical coupling of the as such large rotating mass, i.e. turbine blades and generator. PV units produce direct current, have no rotating mass and are grid-connected via DC-AC inverters.

The increasing share of inverter-based power generation and the associated displacement of usually large-scale and fully controllable generation units and their rotational masses, has the following consequences:

1) The pool of suitable conventional power plants for providing traditional control reserve power is significantly diminished.

2) The rotational inertia of power systems becomes thus markedly time-variant and is reduced, often non-uniformly within the grid topology. Potentially, this leads to new frequency instability phenomena in interconnected power systems. Frequency and power system stability may be at risk.

Eventually, the changes to these two important power system properties need to be reflected in the design of power system control schemes:

1) *Control reserve power:* The shrinking pool of suitable conventional power plants for control reserve provision and frequency regulation increases the motivation to consider non-conventional power system units, e.g. wind turbines, PV units, battery systems and demand-side management, for the provision of control reserve power. Unlike conventional power plants, many of these units exhibit time-varying availability and stringent, thus flexibility-reducing, operational constraints such as time-variant power and energy storage availability. Traditional P/PI-based frequency control cannot handle operational constraints explicitly. This motivates the need for novel grid control schemes.

2) *Grid rotational inertia:* The decrease of rotational inertia in a power system can be mitigated by increasing the inertia contribution from non-conventional units via so-called inertia mimicking. This is achieved through the proper control of non-conventional units, drawing on an internal or external energy storage. Challenges are the real-time tractability and the stringent operational constraints that need to be respected by any control scheme aiming to provide rotational inertia.

The motivation to adapt the current power system control schemes is increasing with every new inverter-based power unit that is commissioned and, likewise, every conventional generator that is decommissioned. Recent studies show the increasing interest on the impact of variable renewable power units on power systems operation as well as on mitigation options [1], [2].

III. Grid Frequency and Frequency Inertia

Power systems are dynamic systems with a high degree of complexity along several dimensions, i.e. time, space and grid hierarchy. Power system processes extend along several time-scales (milliseconds to yearly seasons), spatial distribution is high (100s-1000s km) and multiple grid hierarchies, i.e. different voltage levels, exist. One main characteristic of power systems is that frequency stability, and hence stable operation, depends on the active power balance, meaning that the total power in-feed minus the total consumption (including systems losses) is kept close to zero. Small local disturbances can evolve into consequences influencing the whole power system, in the worst case ending in cascading faults and black-outs. Regarding active power balance, the key system state to observe and control is the grid frequency f (in power systems with several grid control zones also tie-line power exchanges). Grid frequency f is directly coupled to the rotational speed of a synchronous generator ($\omega = 2\pi f$). Deviations from its nominal value, f_0, should be kept small, as damaging vibrations in synchronous machines and load shedding occur in case of larger deviations.
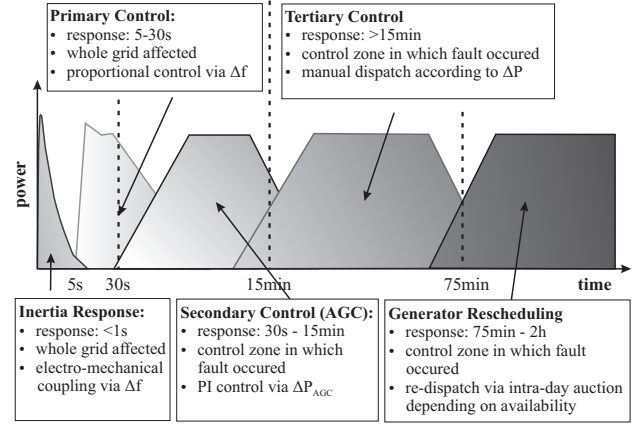

Fig. 1: ENTSO-E frequency control categories [3]–[5].

Maintaining the grid frequency within an acceptable range is thus a necessary requirement for the stable operation of power systems. In normal operation small variations occur spontaneously. Large frequency deviations can be caused by errors in load demand or RES forecasts and the loss of load units, generators or lines.

In the remainder of the paper, regarding frequency control categories etc. we will refer exclusively to the grid code specifications of the ENTSO-E, as defined in [3], for the European continental grid, one of the world's largest synchronous power systems. Here, the nominal grid frequency f_0 is set to be 50 Hz. Please note, that classifications of other power systems usually differ.

Stable power system operation is provided by traditional frequency control, which in [3] has three categories (Fig. 1): Primary frequency control is provided within a few seconds after the occurrence of a frequency deviation. It provides power output proportional to the deviation (P control), stabilizing the system frequency but not restoring it to f_0. Generators of all grid control zones are participating in primary control. The responsible units in the control zone of the imbalance start to take over after approximately 30 s, providing secondary frequency control. As secondary control has an integral control part (PI control), it restores both the grid frequency from its residual deviation and the corresponding tie-line power exchanges with other control zones to the set-point values. Tertiary frequency control manually adapts the power generation set-points and coordinates the power production operation beyond the initial 15 min. time-frame after a fault has occurred. Additionally, generator rescheduling is manually activated according to the expected residual fault in order to relieve tertiary control by cheaper sources at a later stage (i.e. 75 min.) [3]–[5].

This traditional categorization is missing an important contributor to frequency stability: the inertial response, a stabilizing quality of a power system to counteract sudden imposed changes to the grid frequency. The contribution of inertia is an inherent feature of rotating synchronous generators. Due to electro-mechanical coupling, kinetic energy stored in a generator's rotating mass is provided to the grid in case of a frequency deviation.

Figure 2 illustrates the dynamic response of the un-controlled IEEE 14-bus test system to power balance deviations for several inertia setups, representing different shares of conventional generation units. Here, the $\Delta f_{100\%}$ graph shows the behavior of a system, in which only conventional generators are dispatched ($100\% \, H_0$). The other graphs illustrate the system dynamics for decreasing inertia levels (80%, 50% and 20% of H_0). Note, that the rotational inertia H is inversely related to the share of inverter-connected units, which do not contribute to the inertial response.

In general, frequency dynamics are faster for low-inertia power dispatch setups. For the triangle-wave disturbance, Δf and also $\Delta \dot{f}$ are larger for grid setups with lower rotational inertia. The maximum frequency deviation for the step change is the same for all setups but the duration to reach this post-fault steady-state frequency differs significantly. This highlights the importance of the inertial response for power systems as frequency fault dynamics may become too fast for existing frequency control schemes. Hence the value of rotational inertia for shaping frequency dynamics in power systems with high-shares of inverter-connected units is high.
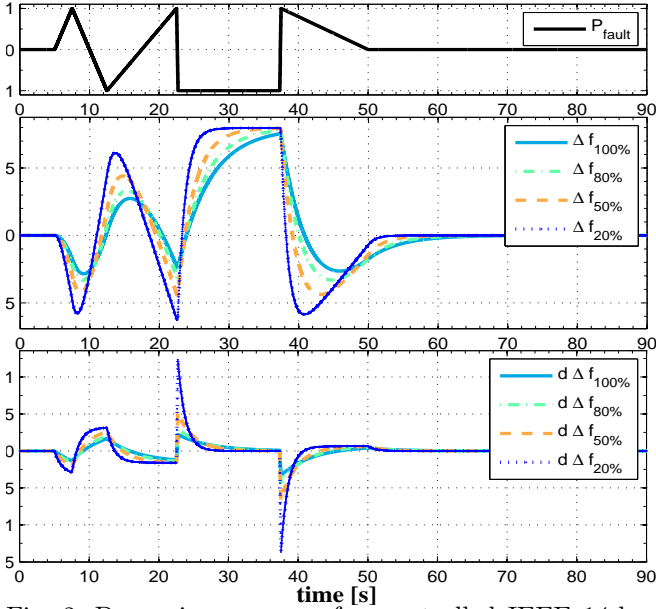

Fig. 2: Dynamic response of uncontrolled IEEE 14-bus system with different inertia ($20 - 100\% \, H_0$) to faults.

A. Inertial Response of a Power System

The derivation of the inertial response follows the line of thought described in [6]. Following a frequency deviation, kinetic energy stored in the rotating masses of the generator system is released, rendering power system frequency dynamics slower and, hence, easier to regulate. The rotational energy is given as

$$E_{\mathrm{kin}} = \frac{1}{2} J (2\pi f_{\mathrm{m}})^2 \quad , \qquad (1)$$

with J as the moment of inertia of the machine and f_{m} the rotating frequency of the machine. The inertia

constant H for a synchronous machine is defined by

$$H = \frac{E_{\mathrm{kin}}}{S_{\mathrm{B}}} = \frac{J(2\pi f_{\mathrm{m}})^2}{2 S_{\mathrm{B}}} \quad , \qquad (2)$$

with S_{B} as the rated power of the generator and H denoting the time duration during which the machine can supply its rated power solely with its stored kinetic energy. Typical values for H are in the range of 2–10 s [7, Table 3.2]. The classical swing equation, a well-known model representation for synchronous generators, describes the inertial response of the synchronous generator as the change in rotational speed ω_{m} (or rotational frequency $f_{\mathrm{m}} = \frac{\omega_{\mathrm{m}}}{2\pi}$) of the synchronous generator following a power imbalance as

$$\dot{E}_{\mathrm{kin}} = J(2\pi)^2 f_{\mathrm{m}} \cdot \dot{f}_{\mathrm{m}} = \frac{2 H S_{\mathrm{B}}}{f_{\mathrm{m}}} \cdot \dot{f}_{\mathrm{m}} = (P_{\mathrm{m}} - P_{\mathrm{e}}) \quad , \quad (3)$$

with P_{m} as the mechanical power supplied by the generator and P_{e} the electric power demand.

Noting that frequency excursions are usually small deviations around the reference value, we replace f_{m} by f_0, and complete the classical swing equation by adding frequency-dependent load damping, a self-stabilizing property of power systems, by formulating

$$\dot{f}_{\mathrm{m}} = -\frac{f_0}{2 H S_{\mathrm{B}} D_{\mathrm{load}}} f_{\mathrm{m}} + \frac{f_0}{2 H S_{\mathrm{B}}} (P_{\mathrm{m},0} - P_{\mathrm{e}} + P_{\mathrm{add}}) \quad . \quad (4)$$

Here f_0 is the reference frequency and D_{load} denotes the frequency-dependent load damping constant. $P_{\mathrm{m},0}$ is the nominally scheduled mechanical generator power. P_{add} denotes additional power in-feed via a generic control loop, providing frequency regulation or inertia provision.

The high share of conventional generators is translated into a large rotational inertia of the here presented interconnected power system. The higher the inertia constant H of the system, the slower are grid frequency dynamics, i.e. the smaller are frequency deviations f_m and its derivative $\Delta \dot{f}_m$ during identical power imbalance faults. With an increasing penetration of non-conventional inverter-connected power units, the frequency inertia of power systems is reduced. This is notably a concern for small power networks, e.g. island grids such as Ireland, with a high share of generation capacity not contributing any inertia. Frequency stabilization becomes thus more difficult. Appropriate adaptations of grid codes are needed.

B. Concept of Inertia Mimicking

Inertia Mimicking (IM) is a control concept that enables inverter-connected generation units to rapidly change their power output, via internal or external power sources, in order to emulate the dynamic response of conventional, rotating generators to frequency variations. For this purpose a control loop is added to the generator bus (Fig. 3), which mimics the characteristics of the conventional generator response as given by its swing equation (Eq. 4) by timely providing otherwise missing kinetic energy. The control scheme providing *virtual*

rotational inertia has to be based on the time-derivative of the swing equation

$$\ddot{f}_{\mathrm{m}} = -\frac{f_0}{2HS_{\mathrm{B}}D_{\mathrm{load}}}\dot{f}_{\mathrm{m}} + \frac{f_0}{2HS_{\mathrm{B}}}(\dot{P}_{\mathrm{m},0} - \dot{P}_{\mathrm{e}} + \dot{P}_{\mathrm{add}}) \ . \quad (5)$$

The control input for correcting the response of the system state $\dot{f}_{\mathrm{m}}$ is $\dot{P}_{\mathrm{add}}$, which is internally integrated before it is applied to the power system as P_{add}.

C. Model Setup of Simulation Cases

An aggregated swing equation model of the well-known IEEE 14-bus test system, which represents a small interconnected power system [8], is used for all presented simulation cases. The disturbance signal – a combination of triangle-wave and step signals – is introduced to the power system (Fig. 2). The triangle-wave signal represents a slow variability in the power balance, e.g. a variation in power in-feed or load demand forecasts, whereas the step signals can be seen as a sudden disturbance, e.g. load or generator disconnection.

Reformulating the classical swing equation (Eq. 4) for a power system with n generators, j loads and l lines, leads to the Aggregated Swing Equation (ASE)

$$\dot{f} = -\frac{f_0}{2HS_{\mathrm{B}}D_{\mathrm{load}}}f + \frac{f_0}{2HS_{\mathrm{B}}}(P_{\mathrm{m}} - P_{\mathrm{load}} - P_{\mathrm{loss}}) \ , \quad (6)$$

with

$$f = \frac{\sum_{i=1}^{n} H_i f_i}{\sum_{i=1}^{n} H_i}, \ S_{\mathrm{B}} = \sum_{i=1}^{n} S_{\mathrm{B},i}, \ H = \frac{\sum_{i=1}^{n} H_i S_{\mathrm{B},i}}{S_{\mathrm{B}}},$$

$$P_{\mathrm{m}} = \sum_{i=1}^{n} P_{\mathrm{m},i}, \ P_{\mathrm{load}} = \sum_{i=1}^{j} P_{\mathrm{load},i}, \ P_{\mathrm{loss}} = \sum_{i=1}^{l} P_{\mathrm{loss},i} \ .$$

Here f is the center of inertia (COI) grid frequency, H the aggregated inertia constant of the n generators, S_{B} the total rated power of the generators, P_{m} the total mechanical power of the generators, P_{load} the total system load of the grid, P_{loss} the total transmission losses of the l lines making up the grid topology and $f_0 = 50$ Hz. The term D_{load} is the frequency damping of the system load [5], which is assumed here to be constant and uniform. The power system parameters used in all simulations are $H = H_0 = 8\,\mathrm{s}$, $S_{\mathrm{B}} = 1.8\,\mathrm{p.u.}$, $D_{\mathrm{load}} = 0.02\,\frac{\%}{\%}$ and $f_0 = 50\,\mathrm{Hz}$. The sampling time $T_{\mathrm{s}} = 20\,\mathrm{ms}$.

The ASE (Eq. 6) is valid for a highly meshed grid, in which all units can be assumed to be connected to the same grid bus, representing the center of inertia of the given grid. Since load-frequency disturbances are normally relatively small, linearized swing equations with $\Delta f_i = f_i - f_0$ can be used. Considering the system change (Δ) before and after a disturbance, the relative formulation of the ASE, assuming that $\Delta P_{\mathrm{loss}} = 0$, is

$$\Delta\dot{f} = -\frac{f_0}{2HS_{\mathrm{B}}D_{\mathrm{load}}}\Delta f + \frac{f_0}{2HS_{\mathrm{B}}}(\Delta P_{\mathrm{m}} - \Delta P_{\mathrm{load}}). \quad (7)$$

An illustration of the general simulation setup with the employed ASE power system models for frequency regulation and grid inertia provision is given in Fig. 3. For

the case of grid inertia provision, the inertial response of a "low-inertia' ASE model (upper model block) initialized with a 80%-inertia setup (i.e. $\sim 20\%$ of generation capacity is inverter-connected) is shaped via another power path in order to mimic, ideally exactly, the behavior of a "high-inertia" ASE power system model (middle model block) with 100% of conventional generation units. For the case of frequency regulation, the additional power path is used for providing frequency regulation. An additional "low-inertia" ASE model (lower model block) is employed as a reference of the dynamic behavior.
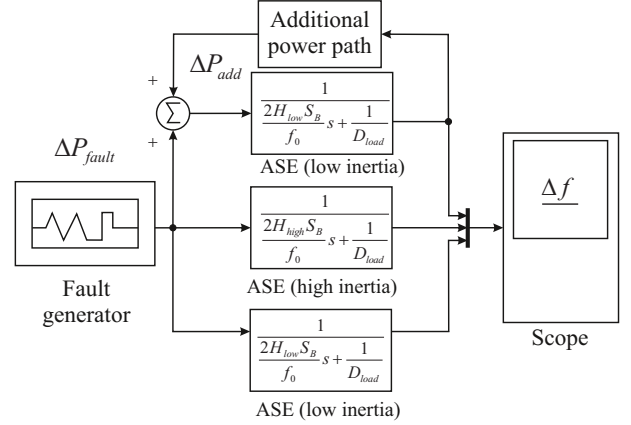

Fig. 3: General simulation setup for inertia provision.

IV. MODEL PREDICTIVE CONTROL

Model Predictive Control (MPC) is often used for problems where its capability to handle system state and control input constraints explicitly is of value. An MPC scheme determines the optimal open-loop response to a system for each time step, as it predicts the future system behavior based on an internal model of the plant dynamics of the controlled system [9].

The internal system model has a decisive role for the performance of MPC schemes. The complexity of the controlled system and, thus, its modeling representation is directly affecting the necessary computational effort. In consequence, the chosen model must be capable of capturing the process dynamics so as to precisely predict the future outputs as well as being simple enough to be implementable. The relatively high computational effort compared with classical PID control schemes has been a barrier for MPC implementation in the past [9].

A. MPC Setup Definition

MPC is formulated as a repeated online solution of a finite horizon open-loop optimal control problem. The problem is to stabilize the linear discrete-time system

$$\begin{aligned} x(k+1) &= Ax(k) + Bu(k) \quad (8) \\ y(k) &= Cx(k) + Du(k) \ , \end{aligned}$$

with the control input $u \in \mathbb{R}^g$, the system state $x \in \mathbb{R}^n$, $y \in \mathbb{R}^f$ the system output, the linear system matrices $A \in \mathbb{R}^{n \times n}$, $B \in \mathbb{R}^{n \times g}$, $C \in \mathbb{R}^{f \times n}$ and $D \in \mathbb{R}^{f \times g}$ at

the discrete time instant $k \in \mathbb{N}$. Using the initial system state measurement $x(0) = [x_1(0), \ldots, x_n(0)]^T = x_0$, a control input u is determined over the prediction horizon $T_\mathrm{p} = N \cdot T_\mathrm{s}$, by solving the optimal control problem

$$\min_{u(\cdot)} \sum_{k=t}^{t+(N-1)} \|Q_x x(k)\|_l + \|Ru(k)\|_l + \|R_\delta \delta u(k)\|_l \quad (9)$$

$$\text{s.t.} \begin{cases} x(k+1) = Ax(k) + Bu(k), \; x_0 = x(0) \;, \\ x_\mathrm{min} \leq x(k) \leq x_\mathrm{max} \;, \\ u_\mathrm{min} \leq u(k) \leq u_\mathrm{max} \;, \\ \delta u_\mathrm{min} \leq \delta u(k) \leq \delta u_\mathrm{max} \;, \end{cases}$$

where $u^* := [u(k)^T, \ldots, u(k+N-1)^T]^T \in R^{g \times N}$ is the resulting optimization vector of the above problem, consisting of the optimal control trajectory of the control inputs for each step of the prediction horizon $k = 0, \ldots, N-1$, with Q_x weighing the state vector $x(t)$, R as the cost term for the control input $u(k)$ and consequently R_δ the cost term for the slew rate of the control input, $\delta u(k) = u(k) - u(k-1)$.

The term l in $\|\cdot\|_l$ specifies the norm of the cost function as $l \in \{1, 2, \infty\}$. Here, the L_2-norm is used throughout. For a given regulation task, constraints can be imposed on the state vector $x(k)$, on the control signal $u(k)$, and on the slew rate of the control input $\delta u(k)$, restricting the solution space to permissible regions. Further cost terms, e.g. a terminal state-constraint, $\|Q_x^\mathrm{term} x(N)\|_l$, can be added to Eq. 9.

Due to uncertainties in the system, e.g. model plant mismatches or disturbances, the optimal control trajectory does not result in the ideal system reaction described by the system model at the end of the prediction horizon. The actual system behavior will be different from the predicted behavior. To react to disturbances and mismatches, feedback on the actual development is incorporated by the receding horizon scheme. MPC schemes of the form shown by Eq. 9 possess no naturally guaranteed closed-loop stability. Stability can be guaranteed via additional terms, i.e. stability constraints, in the setup.

B. Explicit MPC

In the past, real-time applicability of standard online MPC optimizations was limited to simple, low-dimensional problems or systems with slow dynamics.

As frequency control and especially frequency inertia provision should ideally be accomplished very fast and since modern battery systems are in fact able to react fast, i.e. within milliseconds, the motivation for real-time tractability of the employed control scheme is high. In an ideal world, frequency control should be provided with a sampling rate that corresponds to one cycle of the grid frequency, i.e. 20 ms for a grid frequency of 50 Hz. This is also about the sampling rate that robust measurements of grid frequency need [10]. Rotational inertia should be provided on the same time-scale in order to shape the immediate dynamic response of a power system after a

fault, which can be decisive as insufficient inertia may lead to *first swing instability* in a power system [5], [7].

Such fast control response times can be ensured via the offline computation of all possible online control moves using explicit MPC techniques [11], which is well applicable for linear, hybrid systems of a manageable size, i.e. systems that are sufficiently small. The explicit optimization problem pre-computes optimal control laws over all feasible states and stores them in a look-up table, thus effectively shifting most of the computational effort offline. For linear time invariant (LTI) systems the result of this offline calculation of an explicit linear MPC control law has the form

$$u_j(x) = K_j(x) + C_j \,, \text{ with } x \in P_j \subset \Omega_i \;, \quad (10)$$

where $x \in \mathbb{R}^n$ represents the system state and $u_j \in \mathbb{R}^m$ is the optimal control input for the region P_j defined within the sub-space partition Ω_i of the state-space. The MPC setup parameters, e.g. constraints and weights on the states, play an important role with respect to the complexity of the explicit MPC controller solution. The employed prediction horizon N further has an exponential influence on the necessary offline computational cost.

Recent advances in MPC implementation and solver design have drastically reduced computation times, allowing the development of very fast online MPC controllers, see overview and performance comparison in [12].

Nevertheless, explicit MPC retains key advantages for practical implementation. First, feasibility within a pre-defined state-space is guaranteed as all control laws have been computed beforehand. Second, the online computation merely consists of search operations in a look-up table of control laws, hence significantly reducing the computation and storage requirements of controller hardware and significantly speeding up sampling time. The resulting look-up table can furthermore be approximated with satisfactory accuracy into a single polynomial control law, allowing even faster implementation times for practical control problems ($\ll 1\,\mathrm{ms}$) [13].

V. MPC-based Grid Frequency Control and Rotational Inertia Provision

We show that model-based optimal control theory provides the methods for designing control schemes that can provide frequency control or rotational inertia, or both, from *any* generic power system unit, i.e. generators, storages or loads, of which only the relevant operational constraints, categorized by the flexibility metrics power rating (π), power ramp rate (ρ), and energy storage rating (ϵ), need to be known [14], [15]. Control operation is confined to the flexibility volume spanned by these three metrics. The optimal control trajectory may not only be shaped by the control objective itself but also by other considerations, e.g. minimizing operation costs or battery degradation.

Two MPC-based control schemes are presented, first, for performing "conventional" frequency control and, se-

cond, for mimicking frequency inertia of conventional generators. Frequency control aims at the reduction of frequency deviations ($\min_u \Delta f$), while inertia provision increases the inertial response by reducing the frequency rate of change ($\min_u \Delta \dot{f}$). Increasing inertia, indirectly, also leads to a reduction of frequency deviations.

The structure of the control problem is similar for both approaches: the swing equation in its normal form (Eq. 4) as well as its derived form (Eq. 5) is used.

A. MPC-based Frequency Control (FC)

The frequency control (FC) approach uses the directly available system output Δf as control signal. The control input is the regulation power P_{add} that is supplied to the power system through an additional power source, e.g. a generator, load, battery or other energy storage unit. To account for energy constraints in the case of storage units, the additional system state E_{add} is introduced as

$$E_{\mathrm{add}} = \int P_{\mathrm{add}} dt = C_{\mathrm{bat}} \int \dot{x}_{\mathrm{SOC}} dt = C_{\mathrm{bat}} x_{\mathrm{SOC}}, \quad (11)$$

with C_{bat} as the capacity of the additional power source and the limits of the state-of-charge (SOC) x_{SOC} being $+1$ (full), and -1 (empty). The initial setting $x_{\mathrm{SOC}}(0) = 0$ allows control action in both directions.

The MPC FC control problem is defined as follows

$$\dot{\mathbf{x}} = \underbrace{\begin{bmatrix} -\frac{f_0}{2H_{\mathrm{low}}S_B D_{\mathrm{load}}} & 0 \\ 0 & 0 \end{bmatrix}}_{\mathbf{A}} \underbrace{\begin{bmatrix} \Delta f \\ x_{\mathrm{SOC}} \end{bmatrix}}_{\mathbf{x}} + \underbrace{\begin{bmatrix} \frac{f_0}{2H_{\mathrm{low}}S_B} \\ \frac{1}{C_{\mathrm{bat}}} \end{bmatrix}}_{\mathbf{B}} \mathbf{u}$$

with the control input $\mathbf{u} = u = P_{\mathrm{add}}$, and

$$\mathbf{y} = \underbrace{\begin{bmatrix} 1 & 0 \\ 0 & C_{\mathrm{bat}} \end{bmatrix}}_{\mathbf{C}} \underbrace{\begin{bmatrix} \Delta f \\ x_{\mathrm{SOC}} \end{bmatrix}}_{\mathbf{x}} = \begin{bmatrix} \Delta f \\ E_{\mathrm{add}} \end{bmatrix}.$$

The MPC cost function weights are defined as

$$Q_{\mathrm{FC}} = \begin{bmatrix} 10 & 0 \\ 0 & 0 \end{bmatrix}, \quad Q_{\mathrm{FC}}^{\mathrm{term}} = \begin{bmatrix} 0 & 0 \\ 0 & 5e^3 \end{bmatrix},$$

and $R_{\mathrm{FC}} = 1e^{-3}$ and $R_{\delta, \mathrm{FC}} = 2$ with $N = 5$.

Figure 4 shows the system response of the FC strategy. In the top plot the fault signal is depicted. The second plot shows the frequency deviation of the high inertia system (dash), the controlled low-inertia system (solid) and the uncontrolled low-inertia reference system (dash-dot). The third plot shows the time derivative of the frequency deviation (same color coding). The control inputs, P_{add} (π), ΔP_{add} (ρ) and E_{add} (ϵ), are shown in the lower three subplots (4-6), respectively. *Please note, this plot structure will also be maintained for Fig. 5–7.*

The frequency-controlled aggregated power system (FC-SOC 0.25) shows, as expected, a significant reduction of the frequency deviation. For the triangle-wave signal the frequency deviation is reduced by $\approx 80\%$ compared to the non-controlled high inertia reference system. At the beginning of the step fault ($t = 22.5\,\mathrm{s}$) the controller

continues to reduce the frequency deviation until the E_{add} limit is reached ($t = 26.8\,\mathrm{s}$) and no further imbalance power can be absorbed until the reverse step event ($t = 37.5\,\mathrm{s}$). The controller performs well while obeying the defined operational constraints

$$
\begin{array}{llcccl}
\rho : & -1.00\,\mathrm{p.u.} & \leq & \dot{P}_{\mathrm{add}} & \leq & 1.00\,\mathrm{p.u.} \quad, \\
\pi : & -0.10\,\mathrm{p.u.} & \leq & P_{\mathrm{add}} & \leq & 0.10\,\mathrm{p.u.} \quad, \quad (12) \\
\epsilon : & -0.25\,\mathrm{p.u.} & \leq & E_{\mathrm{add}} & \leq & 0.25\,\mathrm{p.u.} \quad.
\end{array}
$$

Furthermore, the frequency deviation shall not exceed $\Delta f \pm 0.50\,\mathrm{Hz}$. The second FC control scheme, using twice the storage capacity (FC-SOC 0.50), has an improved performance during the step faults.
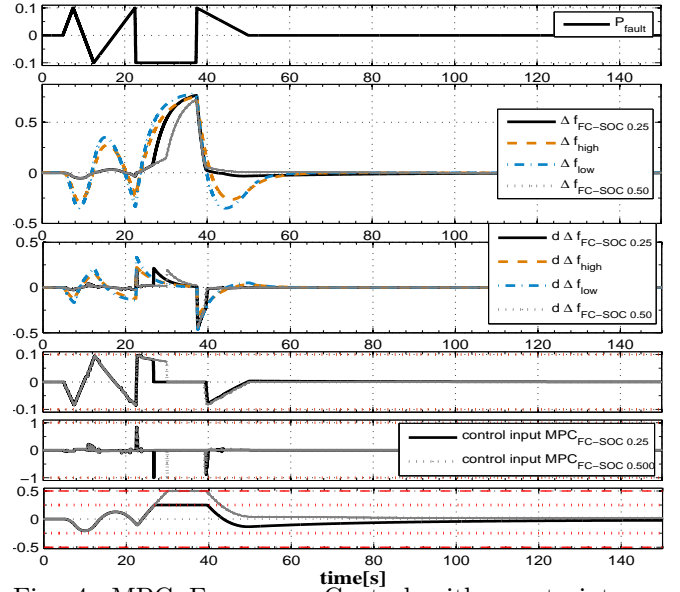

Fig. 4: MPC Frequency Control with constraints on power rating (π), ramp rate (ρ) and energy rating (ϵ).

B. MPC-based Inertia Mimicking (IM)

The setup for inertia mimicking (IM) is more complex than for frequency control (FC). The MPC-based IM control scheme reacts to $\Delta \dot{f}$. The power system output Δf therefore has to be time-differentiated. $\Delta \dot{f}$ is then the input $y_1 = x_1$ to the IM control scheme, whereas the direct output u will be the derivative of the additional power ($\dot{P}_{\mathrm{add}}$). By internally integrating u, the second state x_2 is created, which is the desired control input P_{add}. The third state is similar to the control for frequency control: it formulates the energy constraint E_{add}. The model structure is thus augmented by one state, somewhat increasing the controller complexity.

The MPC IM control problem is defined as follows

$$\dot{\mathbf{x}} = \underbrace{\begin{bmatrix} -\frac{f_0}{2H_{\mathrm{low}}S_B D_{\mathrm{load}}} & 0 & 0 \\ 0 & 0 & 0 \\ 0 & \frac{1}{C_{\mathrm{bat}}} & 0 \end{bmatrix}}_{\mathbf{A}} \mathbf{x} + \underbrace{\begin{bmatrix} \frac{f_0}{2H_{\mathrm{low}}S_B} \\ 1 \\ 0 \end{bmatrix}}_{\mathbf{B}} \mathbf{u},$$

with the control input $\mathbf{u} = u = \dot{P}_{\mathrm{add}}$, which is integrated

and then applied as $\int u\,dt = P_{\mathrm{add}}$, and

$$\mathbf{y} = \underbrace{\begin{bmatrix} 1 & 0 & 0 \\ 0 & 1 & 0 \\ 0 & 0 & C_{\mathrm{bat}} \end{bmatrix}}_{\mathbf{C}} \underbrace{\begin{bmatrix} \Delta\dot{f} \\ P_{\mathrm{add}} \\ x_{SOC} \end{bmatrix}}_{\mathbf{x}} = \begin{bmatrix} \Delta\dot{f} \\ P_{\mathrm{add}} \\ E_{\mathrm{add}} \end{bmatrix}.$$

The MPC cost function weights are defined as

$$Q_{\mathrm{IM}} = \begin{bmatrix} 20 & 0 & 0 \\ 0 & 1e^{-3} & 0 \\ 0 & 0 & 10 \end{bmatrix}, \; Q_{\mathrm{IM}}^{\mathrm{term}} = \begin{bmatrix} 0 & 0 & 0 \\ 0 & 0 & 0 \\ 0 & 0 & 2e^4 \end{bmatrix},$$

and $R_{\mathrm{IM}} = 2$ and $R_{\delta,\,\mathrm{IM}} = 0$ with $N = 5$ and a sampling time of $T_{\mathrm{s}} = 20\,\mathrm{ms}$. The operational constraints are the same as before (Eq. 12).

The fault signal P_{fault} and the resulting frequency rate of change $\Delta\dot{f}$ causes the control scheme to provide additional power to the power system, effectively reducing $\Delta\dot{f}$ (Fig. 5). During the initial triangle-wave signal, this reduction of $\Delta\dot{f}$ also shifts the local maxima in the plots of frequency and frequency derivative, showing the increase of rotational inertia. The step change causes the IM controller to react until the energy limit is reached ($t = 28\,\mathrm{s}$). By changing the capacity of E_{add} (Fig. 5: IM-SOC 0.50) controller saturation can be avoided.
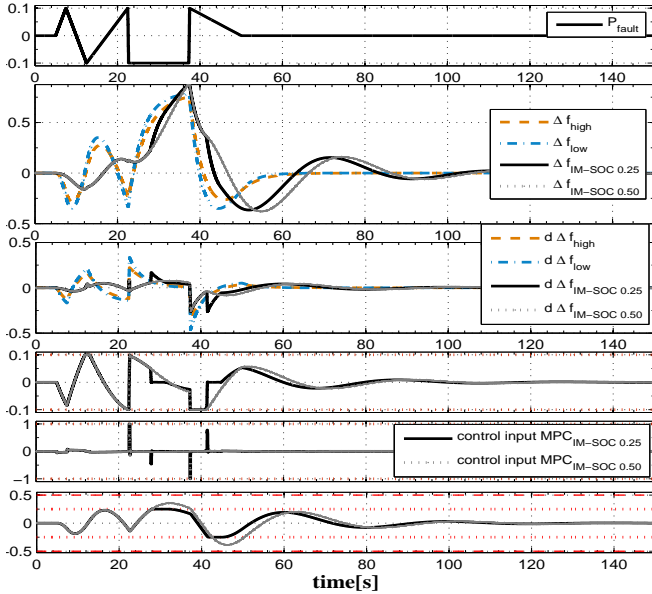

Fig. 5: MPC Inertia Mimicking with constraints on power rating (π), ramp rate (ρ) and energy rating (ϵ).

C. Combined Frequency Control and Inertia Mimicking versus Traditional P/PI-based Frequency Control

This section builds upon the aforementioned scenarios and compares the performance of three different control setups: (a) the traditional primary and secondary frequency control (droop control [P] and AGC [PI]) with and without limits (trad FC limited and trad FC), (b) the MPC-based frequency controller as described in Section V-A (MPC$_{\mathrm{FC}}$), and (c) the combination of both the MPC-based frequency *and* inertia mimicking control

(MPC$_{\mathrm{FC+IM}}$). For the case (c) (Fig. 6), the two controllers FC MPC$_{\mathrm{FC+IM}}$ and IM MPC$_{\mathrm{FC+IM}}$ are connected in parallel, controlling two separate energy sources (E_{add}). A fourth case is also plotted, showing the frequency deviation, as well as the time derivative of frequency deviation, for the non-controlled low inertia setup (low). All ASE use the "low-inertia" setup, i.e. 80% conventional generators. The setup for the MPC controllers is identical to Section V. Details on traditional AGC schemes can be found in [16, Ch. 5.1.3, Appendix B].

The two MPC controllers outperform the traditional frequency control, as long as they are active (Fig. 7), i.e. while no saturation limits are reached. Due to their limited energy capacity E_{add}, the two MPC-FC's control inputs are zero during $t = 30 - 45\,\mathrm{s}$ for FC MPC$_{\mathrm{FC+IM}}$ and during $t = 30 - 35\,\mathrm{s}$ for MPC$_{\mathrm{FC}}$. For this duration, the frequency deviation is higher compared to the unconstrained traditional frequency control (*trad FC*). The traditional frequency control with energy constraint (*trad FC limited*) also causes the control to be inactive for $t = 36 - 39\,\mathrm{s}$. Note that the energy constraint plot (lowest sub-figure) depicts the combined energy consumption of MPC$_{\mathrm{FC+IM}}$ (black graph) for which the energy constraint (ϵ) is at ± 1.0 (instead of ± 0.5). The plot further shows that for the time-frame from $t = 45\,\mathrm{s}$ till $t = 60\,\mathrm{s}$, the two control inputs P_{add} of FC MPC$_{\mathrm{FC+IM}}$ and P_{add} of IM MPC$_{\mathrm{FC+IM}}$ counteract each other. This behavior indicates that it is of advantage to realize the combined MPC$_{\mathrm{FC+IM}}$ via an integrated multi-objective MPC FC+IM scheme. However, separating the FC MPC and IM MPC control schemes was a deliberate choice here. The IM MPC scheme shapes the dynamic response of a low-inertia system to look like that of a high-inertia system (Fig. 6). The FC MPC scheme than has to regulate only the slower dynamics of the high-inertia system.

D. Controller Performance and Scalability

Both the FC and IM control schemes are implemented as local control loops, which is similar to existing fast frequency control, i.e. primary frequency control, which reacts to local measurements of Δf and $\Delta\dot{f}$ only, and hence does not necessitate communication or coordination. Therefore, the size of the individual control problems, i.e. size of state $\mathbf{x}$ and control input vector $\mathbf{u}$, is indepen-
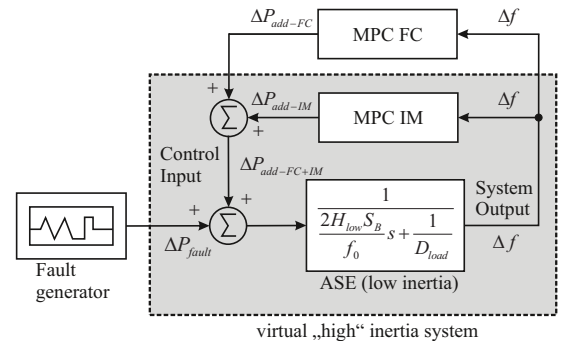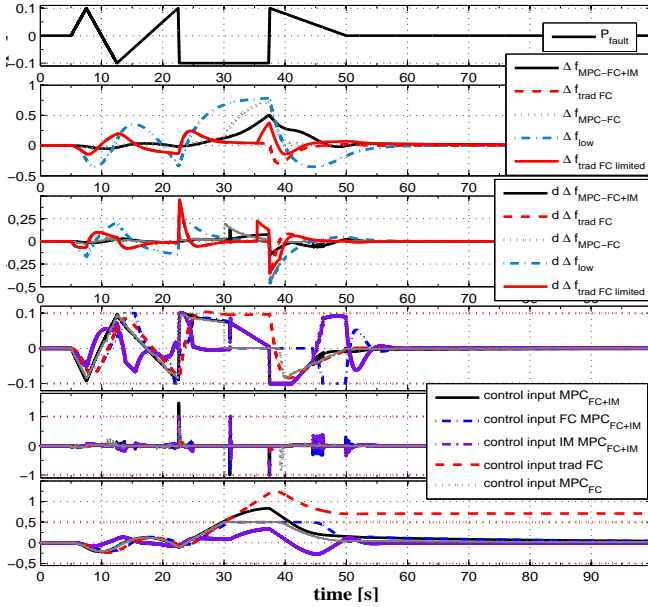

Fig. 6: Scheme of the combined MPC for IM and FC.

Fig. 7: Comparison of conv. frequency control (conv. FC) with MPC-based FC and MPC-based FC+IM.

dent of the power system size (FC: 2 states, 1 input — IM: 3 states, 1 input). The size, and hence complexity, of the MPC setups furthermore depends (exponentially) on the prediction horizon N. Its choice depends indirectly on the time-constant of the frequency dynamics of a given power system, more precisely the local grid parameters at the controller bus, and the sampling time. However, for all our simulation cases, a higher value for N did not result in a better control performance. Realistic values for H and D_{load}, similar also for large interconnected power systems, were chosen for the Aggregated Swing Equation (ASE) model. We do not expect significant differences for the practical application of the here proposed control schemes. The proposed MPC FC and MPC IM controllers should scale well for *any* power system size.

Table I gives an overview of the computational efforts of the here employed FC and IM control schemes. Control performance was similar for online and explicit MPC simulation. The offline computation takes less than 30 s for all presented control schemes, while the full simulation run-time of 200 s length is calculated in less than one second, confirming the real-time capability of the explicit control schemes. Traditional online MPC – with the tools and solvers used here – is too slow and not applicable, especially since in practical application controllers will have to run on embedded systems.

VI. Conclusion & Outlook

We show that there exist meaningful applications for MPC in power systems control, notably for frequency regulation and frequency inertia provision. Compliance with operational constraints of power system units is enforced. Future work investigates the addition of stability constraints and the incorporation of frequency control and inertia provision into one unified control strategy.

TABLE I: Overview of Computational Efforts.

Control strategy	Computation [s]	Simulation [s]	Regions
FC explicit	11.55	0.61	427
IM explicit	18.77	0.28	315
FC+IM explicit	27.52	0.51	742
FC online	3.02	188.96	
IM online	2.98	162.05	
FC+IM online	5.68	374.03	

Hardware: Pentium Dual Core 3 GHz with 3GB RAM.
Calculation: All calculations were performed using the MPT toolbox [17] with the solvers `MP-QP` (explicit MPC) and `QuadProg` (online MPC). Simulations are described in detail in this section.
Assessment: 'Simulation' is the run-time of a Matlab/Simulink simulation of 200 s length ($T_s = 20$ ms); "Computation" is time for offline computation of the explicit controller.

References

[1] J. Morren, S. de Haan, and J. Ferreira, "Contribution of DG units to primary frequency control," in *2005 International Conference on Future Power Systems*, Nov. 2005.

[2] G. Lalor, J. Ritchie, S. Rourke, D. Flynn, and M. O'Malley, "Dynamic frequency control with increasing wind generation," in *IEEE Power Engineering Society General Meeting, 2004*, vol. 2, Jun. 2004, pp. 1715 – 1720.

[3] Union for the Coordination of Transmission of Electricity, *Operation Handbook Appendix 1 - Load-Frequency Control and Performance.* Paris: ENTSO-E/UCTE, www.entsoe.eu.

[4] G. Andersson, C. Alvarez Bel, and C. Cañizares, *Frequency and Voltage Control in Electric Energy Systems.* CRC press, 2009, ch. 9.

[5] G. Andersson, *Dynamics and Control of Electric Power Systems.* ETH Zürich, 2010, Lecture Notes.

[6] J. Morren, J. Pierik, and S. de Haan, "Inertial response of variable speed wind turbines," *Electric Power Systems Research*, vol. 76, no. 11.

[7] P. Kundur, N. Balu, and M. Lauby, *Power system stability and control*, ser. EPRI power system engineering series. New York: McGraw-Hill, 1994.

[8] Power Systems Test Case Archive, College of Engineering, University of Washington. www.ee.washington.edu/research/pstca/.

[9] E. F. Camacho and C. Bordons, *Model predictive control*, ser. Advanced textbooks in control and signal processing. New York: Springer, 2003.

[10] M. Akke, "Some control applications in electrical power systems (phd thesis)," LTH, Dept. of Industrial Electrical Engineering and Automation, Lund, Sweden, 1997.

[11] A. Bemporad, F. Borrelli, and M. Morari, "Explicit solution of LP-based Model Predictive Control," in *Proceedings on the 39th IEEE Conference on Decision and Control*, Sydney, 2000.

[12] A. Domahidi, A. Zgraggen, M. Zeilinger, M. Morari, and C. Jones, "Efficient Interior Point Methods for Multistage Problems Arising in Receding Horizon Control," in *IEEE Conference on Decision and Control*.

[13] A. Ulbig, S. Olaru, D. Dumur, and P. Boucher, "Explicit nonlinear predictive control for a magnetic levitation system," *Asian Journal of Control*, vol. vol. 12, no. 3, p.1-9, May 2010.

[14] A. Ulbig and G. Andersson, "On Operational Flexibility in Power Systems," in *IEEE PES General Meeting, San Diego, USA*, July 2012.

[15] Y. Makarov, C. Loutan, J. Ma, and P. de Mello, "Operational Impacts of Wind Generation on California Power Systems," *Power Systems, IEEE Transactions on*, vol. 24, no. 2, May 2009.

[16] T. Rinke, "MPC-based frequency regulation and inertia mimicking for improved grid integration of renewable energy sources," Master's thesis, ETH Zürich Power Systems Laboratory, 2011, http://www.eeh.ee.ethz.ch/uploads/tx_ethpublications/Rinke_2011.pdf.

[17] M. Kvasnica, P. Grieder, M. Baotić, and F. Christophersen, *Multi-Parametric Toolbox*, ETH Zürich Automatic Control Laboratory, 2006.